Catalysis Letters (2019) 149:2376–2382
https://doi.org/10.1007/s10562-019-02834-3

Free-Standing Porous Cu-Based Nanowires as Robust Electrocatalyst for Alkaline Oxygen Evolution Reaction

Zhihao Li[1] · Xingbo Ge[1] · Zhengnan Wang[1] · Ling Zhang[2] · Luyi Huang[2]

Received: 6 March 2019 / Accepted: 16 May 2019 / Published online: 30 May 2019

Abstract

Cu-based catalysts have emerged as important candidates for oxygen evolution reaction (OER) electrocatalysts. Based on $Mg_{72}Cu_{28}$ alloy ribbon, a free-standing porous Cu hydroxide/oxide nanowires (p-CuNWs) was fabricated by a combined method of chemical dealloying and electrochemical treatment. The structure and chemical state of p-CuNWs were characterized by X-ray diffraction pattern analysis, scanning electron microscopy, and X-ray photoelectron spectroscopy. The p-CuNWs were identified as mixed $Cu(OH)_2$ and CuO with a high active surface area, which exhibit robust activity for OER in alkaline solution with an overpotential of only 377 mV to offer current density of 50 mA cm^{-2}, small Tafel slope of 85 mV dec^{-1}. The catalytic durability of p-CuNWs was also evaluated by cyclic voltammetry cycles and a small decay of activity was observed.

Graphical Abstract

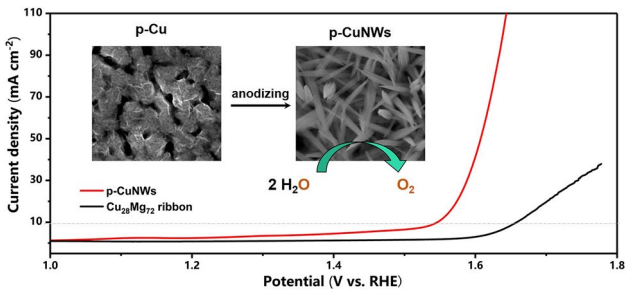

Keywords Cu-based nanowires · Dealloying · Nanostructure · Electrocatalysis · Oxygen evolution reaction

1 Introduction

The exploitation of suitable electrocatalysts with high catalytic activity for oxygen evolution reaction (OER) is a challenging and important topic for hydrogen production from water splitting [1, 2]. Currently, precious metal-based materials, such as IrO_2 [3], RuO_2 [4] and Pd [5] are believed to be state-of-the-art electrocatalysts for OER, which can efficiently drive the OER with low overpotentials. Nevertheless, the industrial-scale applications are constrained by their scarcity and high cost. Hence, numerous efforts have been devoted to fabricate efficient and stable OER catalysts based on earth-abundant metal.

✉ Xingbo Ge
xbge@swpu.edu.cn

✉ Ling Zhang
lzhang@usst.edu.cn

[1] School of Chemistry and Chemical Engineering, Southwest Petroleum University, Chengdu 610500, People's Republic of China

[2] School of Optical-Electrical and Computer Engineering, University of Shanghai for Science and Technology, Shanghai 200093, People's Republic of China

As an abundant and inexpensive metal, copper has a wide range of oxidation states (Cu^0, Cu^+, Cu^{2+} and Cu^{3+}) which makes it suitable for many potential applications [6], including organic transformation [7], electrocatalysis [8], and photocatalysis [9]. Recently, a lot of attention was paid to homogeneous Cu-based catalysts for OER due to their attractive electrocatalytic characteristics [10, 11]. Very recently, heterogeneous Cu-based hydroxides and oxides were also demonstrated as active composites for OER in alkaline media [12–16]. Therefore, there is an increasing interest in the fabrication of Cu-based nanostructures as efficient OER catalysts [17–25]. For example, Pawar et al. reported a two-dimensional CuO nanosheet film electrode, and the excellent OER performance in alkaline solution was realized after a heat treatment [17]. Among the fabricated Cu based catalysts, Cu nanowires achieved remarkable progress in OER due to their high electrical conductivity from the unique structure [18, 19]. Meanwhile, three dimensional porous architectures are often created to further improve the catalytic efficiency, by offering tremendous specific surface area and availability for OER [20–22]. Based on the hydrogen bubble dynamic template method, a series of porous Cu-based nanostructures, including dendritic Cu oxide [20], Cu_2O–Cu hybrid foams [21], CuO/C hollow shell@Cu dendrites [22], have been fabricated and their enhanced OER activities have been confirmed.

In the past decade, chemical/electrochemical dealloying has been emerging as a promising approach to fabricate free-standing porous materials for electrocatalysis [26–29]. Dealloying ribbon or film precursor often generates a free-standing porous structure extending in three dimensions, which is highly desirable for free transport of medium molecules. In addition, a free-standing catalyst can largely minimize the complexity of fabrication process and completely eliminate the resistance between the support and the active ingredient. Adopting this dealloying strategy, Ding et al. fabricated a series of metal electrocatalysts with free-standing porous structures and their excellent catalytic performances towards many important electrochemical reactions were demonstrated [30–32]. Recently, by carefully designing the alloy precursor and electrochemical dealloying potential, Chen et al. fabricated a nanoporous Co/Fe phosphides with outstanding activity towards both hydrogen evolution and OER [33].

Inspired by the reported free-standing materials as mentioned above, here, we report a free-standing porous Cu-based nanowires (p-CuNWs) fabricated by a combined method of chemical dealloying and electrochemical treatment. The as-fabricated p-CuNWs exhibit excellent activity and offer large current density for OER at a low overpotential in alkaline solution.

2 Experimental

2.1 Fabrication of p-CuNWs

The fabrication procedure of p-CuNWs is illustrated in Fig. 1a. The precursor $Mg_{72}Cu_{28}$ master alloy with nominal compositions were fabricated by arc melting the mixtures of pure Mg (99.99%) and Cu (99.99%) under a high-purity argon gas atmosphere. Subsequently, a melt spinning technique was introduced to re-melted the as-prepared precursor alloy, followed by injection onto a spinning copper roller to obtain the alloy ribbon. The resulting $Mg_{72}Cu_{28}$ ribbon is of thickness ~ 20 μm. The p-Cu was made by dealloying $Cu_{28}Mg_{72}$ ribbon in a 0.68 M HCl solution at 25 °C for 60 s. The p-Cu samples were rinsed in pure water (18.2 MΩ cm) to remove the residual chemical ion impurities. The p-CuNWs were then fabricated from the anode oxidation of p-Cu in 1.0 M KOH on a CHI 660E electrochemical workstation, by performing a linear sweep voltammetry (LSV) from − 0.6 to 0.8 V versus Ag/AgCl with a scan rate of 1 mV/s. The p-Cu was directly used as the working electrode. An Ag/AgCl (sat. KCl) electrode and a Pt wire were employed as the reference electrode and counter electrode, respectively.

2.2 Characterizations

X-ray diffraction (XRD) pattern analysis of as-prepared materials were recorded on an X'Pert Pro MPD (PANalytical, The Netherlands) X-ray diffractometer at room temperature using Cu Kα ($\lambda = 0.154060$ nm) as radiation source (40 kV and 40 mA). The structure and morphology analysis of the p-Cu and p-CuNWs were conducted using scanning electron microscopy (SEM, FEI, Inspect F50) at 10 kV accelerating voltage. X-ray photoelectron spectroscopy (XPS) was performed on a Thermo Fisher Scientific ESCALAB 250 photoelectron spectrometer (Al Kα radiation, $\lambda = 1486.6$ eV).

2.3 Electrochemical Measurement

All electrochemical measurements were performed at room temperature in 1.0 M KOH electrolyte on a CHI 660E electrochemical workstation using a standard three-electrode cell, consisting of as-prepared p-CuNWs or $Mg_{72}Cu_{28}$ as the working electrode, a Pt wire as the counter electrode, and an Ag/AgCl (sat. KCl) as the reference electrode. The OER activities of the samples were determined by LSV with a scan rate of 1 mV s^{-1}. A 90%-iR correction was applied to all of the original data, except when specified otherwise. The potentials reported in the text were converted to the

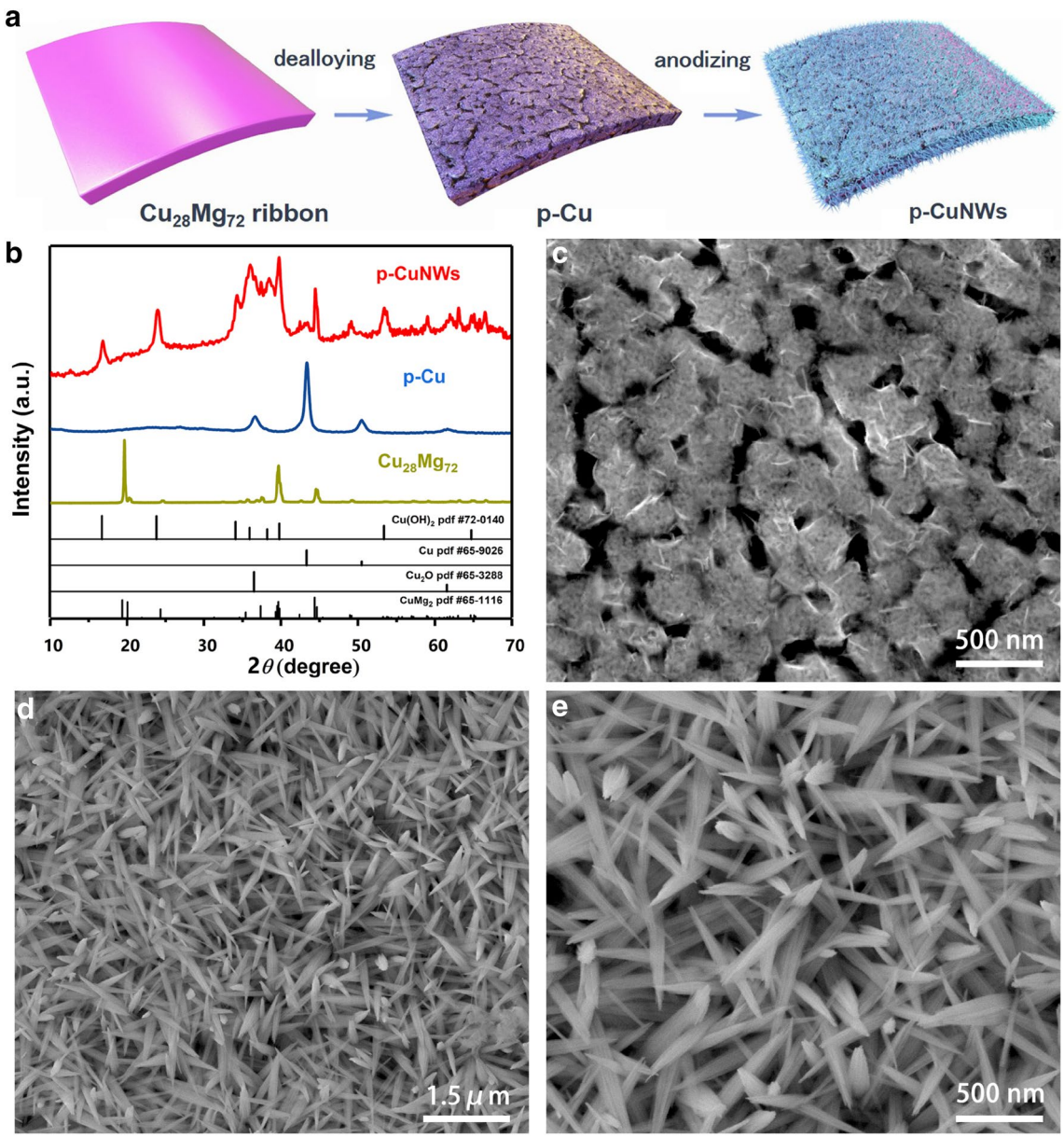

Fig. 1 **a** Schematic description of the fabrication process of p-CuNWs. **b** XRD pattern of p-CuNWs, p-Cu and $Cu_{28}Mg_{72}$ ribbon. **c** SEM image of p-Cu. **d**, **e** SEM images of p-CuNWs with different magnification

reversible hydrogen electrode (RHE) potential according to the equation E(RHE) = E(Ag/AgCl) + 0.059 × pH + 0.197 V. The OER overpotentials (η) were calculated using the equation η = E(RHE) − 1.23 V.

3 Results and Discussion

The XRD patterns (Fig. 1b) demonstrate that the $Cu_{28}Mg_{72}$ ribbons composed primarily of orthorhombic $CuMg_2$ phase (JCPDS No. 65-1116). In addition, several weak diffraction peaks (2θ = 32.4°, 34.6°, 36.8° and 47.9°) are ascribed to metallic Mg (JCPDS No. 01-1141), indicating the bimetallic precursor is a mixture of $CuMg_2$ and Mg. Owing to the disparity in chemical stability of Mg and Cu element, the Mg was selectively and rapidly dissolved from the bimetallic ribbons in a HCl solution, accompanying with vigorous hydrogen gas evolution on the surface of ribbons. After dealloying, the main diffraction peaks at 43.4° and 50.5° of the p-Cu correspond to (111) and (200) planes of Cu (JCPDS No. 65-9026), respectively. The extremely weak peaks at 36.5° and 61.5° indicate the existence of a small quantity of Cu_2O (JCPDS No. 65-3288) resulting from oxidation of surface Cu in atmospheric air. The disappearance of $CuMg_2$ and Mg

peaks is indicative of the dissolution of most the Mg during 60 s dealloying process. For the as-fabricated p-CuNWs, the XRD pattern suggests a mixture of Cu hydroxide/oxide. The diffraction peaks at 16.8°, 24.0°, 34.4° and 39.7° can be indexed to the (020), (021), (002) and (130) planes of orthorhombic $Cu(OH)_2$ (JCPDS No. 72-0140), respectively, and the dominant pattern indicates the high percentage of $Cu(OH)_2$ in p-CuNWs sample. Interestingly, the diffraction peaks of $CuMg_2$, completely suppressed by the strong peaks of Cu in the p-Cu sample, clearly show off in p-CuNWs, indicative of the existence of little residual $CuMg_2$ alloy and the relatively poor crystallinity of $Cu(OH)_2$ as compared to metallic Cu. The additional weak peaks mainly result from a small quantity of CuO (JCPDS No. 03-0867) and residual Cu in p-CuNWs.

SEM images of p-Cu and p-CuNWs are shown in Fig. 1c–e. The p-Cu sample exhibits a porous structure with interconnected pore channels and Cu ligaments with a size of 100 ~ 200 nm (Fig. 1c). The anode oxidation of p-Cu results in the electrochemical generation of dense hydroxide/oxide needle-like nanowires on the surface, as shown in Fig. 1d. The high magnification SEM image (Fig. 1e) shows the nanowires with a uniform diameter of ca. 80 nm. The as-fabricated p-CuNWs exhibits integrated advantages of porous structure and nanowires, proving numerous active sites for OER and improved availability of active species. This in situ direct generation strategy also ensures a decent mechanical adhesion and electric connection to electrocatalysis application.

XPS was used to probe the valence states p-CuNWs, as shown in Fig. 2. The survey spectra shows signals for Cu, O and Mg (Fig. 2a). The weak signals of Mg indicate the low concentration of Mg on the surface. The high resolution of O 1 s spectra (Fig. 2b) could be deconvoluted into two peaks located at about 529.4 and 531.6 eV, corresponding to O^{2-} and OH^- respectively [34, 35]. The high intensity of OH^- signals indicates that p-CuNWs surface is mainly made up of hydroxide. The Cu 2p spectra further confirms this observation, as shown in Fig. 2c. The appearances of the satellite peaks at about 942.9 and 962.8 eV are the evidences of Cu^{2+} [35–37]. The main Cu $2p_{3/2}$ (934.7 eV) and Cu $2p_{1/2}$ (954.6 eV) peaks indicate the Cu^{2+} connects with OH^- [37, 38], in good agreement with the XRD results.

The electrocatalytic OER performance of p-CuNWs was determined in 1.0 M KOH (pH 13.6), as shown in Fig. 3a. While the bare $Cu_{28}Mg_{72}$ alloy has poor catalytic activity for OER, p-CuNWs shows significantly superior catalytic activity and only needs an overpotential as low as 310 mV to drive current density of 10 mA cm^{-2}. To drive 50 and 100 mA cm^{-2}, p-CuNWs only needs an overpotential of 377 and 409 mV, respectively. The observed activity is also superior to the behaviors of most reported Cu-based OER catalysts in alkaline media, including 2D CuO nanosheet

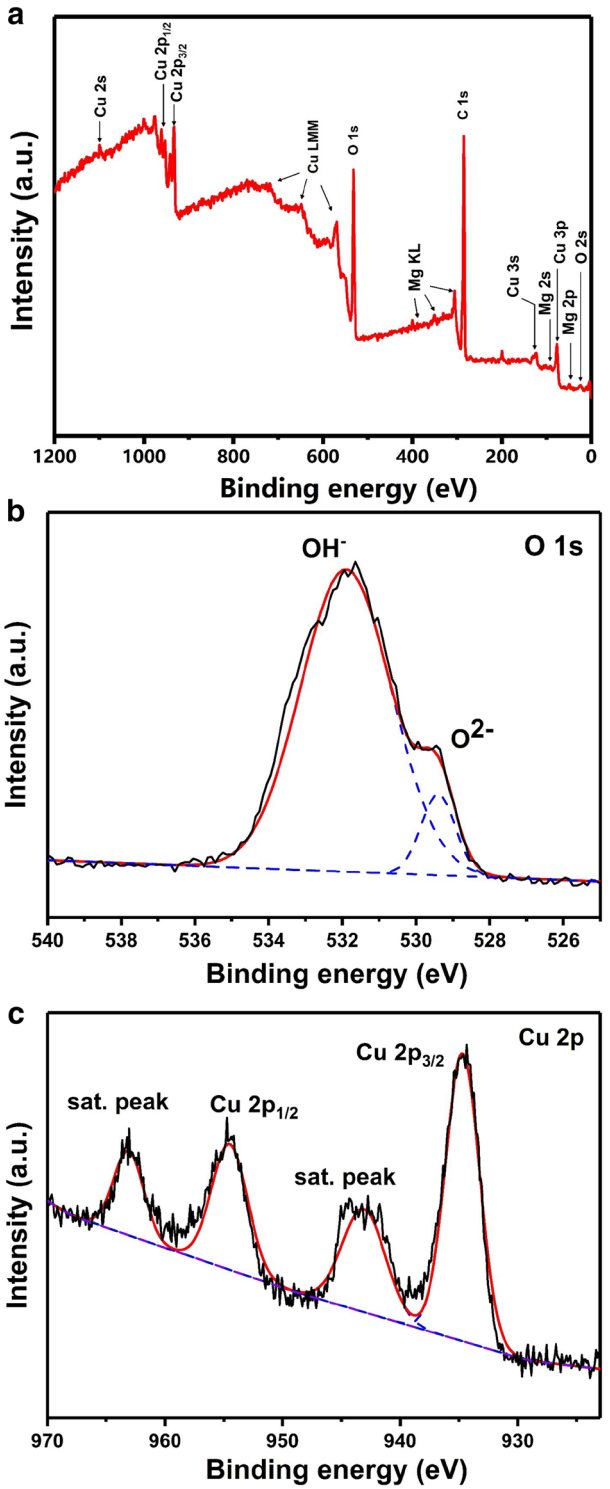

Fig. 2 **a** XPS survey for p-CuNWs, **b** O 1 s and **c** Cu 2p regions

film ($\eta_{10\,mA\,cm^{-2}} = 350$ mV) [17], $Cu(OH)_2$ nanowire arrays ($\eta_{10\,mA\,cm^{-2}} = 430$ mV) [19], Cu_2O-Cu hybrid foams ($\eta_{10\,mA\,cm^{-2}} = 350$ mV) [21]. The enhanced performance of the p-CuNWs could be attributed to the porous nanowire

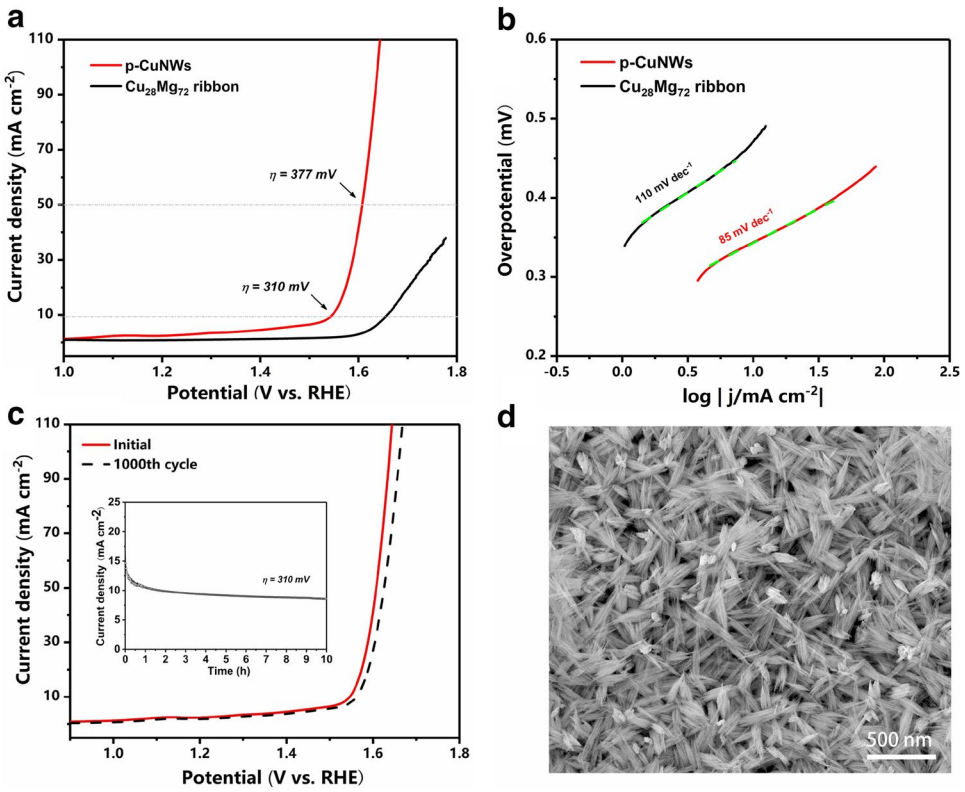

Fig. 3 **a** LSV curves of p-CuNWs and $Cu_{28}Mg_{72}$ ribbon in 1.0 M KOH. **b** The corresponding Tafel plots of p-CuNWs and $Cu_{28}Mg_{72}$ ribbon. **c** OER polarization curves of the p-CuNWs before and after 1000 cycles in 1.0 M KOH (inset: chronoamperometry curves of the p-CuNWs in 1.0 M KOH). **d** SEM image of p-CuNWs after chronoamperometry for 10 h

structure from dealloying and electrochemical treatment. The Tafel slope (Fig. 3b) of p-CuNWs is 85 mV dec^{-1}, indicating that the discharge of OH^- ($M + OH^- \rightarrow M\text{-}OH + e^-$, where "M" denotes the active site) is most likely to be the rate determining step in alkaline conditions [18, 39].

The high catalytic performance of p-CuNWs electrode could be attributed to the Cu hydroxide/oxide nanowires on the surface. It is accepted that OER on oxide surfaces consists of four consecutive electrochemical reactions, and the metal hydroxide/oxide could be oxidized to active intermediate during the reaction process [40, 41]. In our case, the formation of Cu^{III} oxide from Cu hydroxide/oxide at anodic potential is considered as the active intermediate for catalyzing OER, as revealed by in situ Raman spectroscopy on Cu-based catalyst in Yeo group [42, 43]. Meanwhile, the small amount of residue Cu and $CuMg_2$ inside the catalyst provides a high conductivity that facilitates the transport of electron during the catalysis. The free-standing porous structure of p-CuNWs offers a large amount of active surface area and the free transport of medium molecules. All of these features make the p-CuNWs a superior OER catalyst as compared to other Cu-based materials.

Long-term stability of p-CuNWs was also evaluated by continuous cyclic voltammetry (CV) scanning for 1000 cycles in 1.0 M KOH (Fig. 3c). A small decay of activity is observed, indicating the imperfect durability of this material. The durability is further measured by electrolysis at an overpotential of 310 mV over 10 h (Fig. 3c inset). The p-CuNWs electrode exhibits an obvious decay of activity in the first hour, and then the current density keeps at a value of ca. 10 mA cm^{-2}. To explore the reason of the observed activity decay, the surface morphology of p-CuNWs after electrolysis was analyzed by SEM, as shown in Fig. 3d. An observable coarsening and agglomeration of the nanowires occurred during the electrolysis, which may result in the small decay of long-term catalytic performance. Further study could focus on the improvement of the durability of p-CuNWs, and related work on this issue is currently underway.

4 Conclusion

A free-standing Cu-based electrocatalyst was fabricated by chemical dealloying $Mg_{72}Cu_{28}$ alloy ribbon and following electrochemical anodization process. The dissolution of Mg from the alloy during chemical dealloying resulted in a formation of porous Cu, and the following electrochemical anodization process converted most of Cu into Cu hydroxide/oxide nanowires with a uniform diameter of ca. 80 nm. The free-standing structure, high surface area and high porosity makes the as-prepared p-CuNWs a robust catalyst for OER. The p-CuNWs exhibits enhanced OER activity in alkaline solution with an overpotential of only 377 mV to

offer current density of 50 mA cm^{-2}. This work provides a pathway for designing Cu-based 3D architectures electrocatalyst for OER.

Acknowledgements This work was supported by the National Natural Science Foundation of China (21403174).

Compliance with Ethical Standards

Conflict of interests The authors declare that they have no conflict of interest.

References

1. Walter MG, Warren EL, McKone JR, Boettcher SW, Mi QX, Santori EA, Lewis NS (2010) Solar water splitting cells. Chem Rev 110:6446–6473
2. Jiao Y, Zheng Y, Jaroniecb M, Qiao SZ (2015) Design of electrocatalysts for oxygen- and hydrogen-involving energy conversion reactions. Chem Soc Rev 44:2060–2086
3. Dau H, Limberg C, Reier T, Risch M, Roggan S, Strasser P (2010) The mechanism of water oxidation: from electrolysis via homogeneous to biological catalysis. ChemCatChem 2:724–761
4. Audichon T, Napporn TW, Canaff C, Morais C, Comminges C, Kokoh KB (2016) IrO_2 coated on RuO_2 as efficient and stable electroactive nanocatalysts for electrochemical water splitting. J Phys Chem C 120:2562–2573
5. Joya KS, Ehsan MA, Babar NA, Sohail M, Yamani ZH (2019) Nanoscale palladium as a new benchmark electrocatalyst for water oxidation at low overpotential. J Mater Chem A 7:9137–9144
6. Gawande MB, Goswami A, Felpin FX, Asefa T, Huang XX, Silva R, Zou XX, Zboril R, Varma RS (2016) Cu and Cu-based nanoparticles: synthesis and applications in catalysis. Chem Rev 116:3722–3811
7. Decan MR, Impellizzeri S, Marin ML, Scaiano JC (2014) Copper nanoparticle heterogeneous catalytic 'click' cycloaddition confirmed by single-molecule spectroscopy. Nat Commun 5:4612
8. Kas R, Kortlever R, Milbrat A, Koper MTM, Mul G, Baltrusaitis J (2014) Electrochemical CO_2 reduction on Cu_2O-derived copper nanoparticles: controlling the catalytic selectivity of hydrocarbons. Phys Chem Chem Phys 16:12194–12201
9. Wu NL, Lee MS (2004) Enhanced TiO_2 photocatalysis by Cu in hydrogen production from aqueous methanol solution. Int J Hydrogen Energy 29:1601–1605
10. Barnett SM, Goldberg KI, Mayer JM (2012) A soluble copper-bipyridine water-oxidation electrocatalyst. Nat Chem 4:498–502
11. Zhang MT, Chen ZF, Kang P, Meyer TJ (2013) Electrocatalytic water oxidation with a copper(II) polypeptide complex. J Am Chem Soc 135:2048–2051
12. Liu X, Jia HX, Sun ZJ, Chen HY, Xu P, Du PW (2014) Nanostructured copper oxide electrodeposited from copper(II) complexes as an active catalyst for electrocatalytic oxygen evolution reaction. Electrochem Commun 46:1–4
13. Du JL, Chen ZF, Ye SR, Wiley BJ, Meyer TJ (2015) Copper as a robust and transparent electrocatalyst for water oxidation. Angew Chem Int Ed 54:2073–2078
14. Liu X, Cui SS, Sun ZJ, Du PW (2015) Copper oxide nanomaterials synthesized from simple copper salts as active catalysts for electrocatalytic water oxidation. Electrochim Acta 160:202–208
15. Cui SS, Liu X, Sun ZJ, Du PW (2016) Noble metal-free copper hydroxide as an active and robust electrocatalyst for water oxidation at weakly basic pH. ACS Sustain Chem. Eng. 4:2593–2600
16. Joya KS, Groot HJM (2016) Controlled surface-assembly of nanoscale leaf-type Cu-oxide electrocatalyst for high activity water oxidation. ACS Catal 6:1768–1771
17. Pawar SM, Pawar BS, Hou B, Kim J, Ahmed ATA, Chavan HS, Jo Y, Cho S, Inamdar AI, Gunjakar JL, Kim H, Cha S, Im H (2017) Self-assembled two-dimensional copper oxide nanosheet bundles as an efficient oxygen evolution reaction (OER) electrocatalyst for water splitting applications. J Mater Chem A 5:12747–12751
18. Cheng NY, Xue YR, Liu Q, Tian JQ, Zhang LX, Asiri AM, Sun XP (2015) Cu/($Cu(OH)_2$-CuO) core/shell nanorods array: in situ growth and application as an efficient 3D oxygen evolution anode. Electrochim Acta 163:102–106
19. Hou CC, Fu WF, Chen Y (2016) Self-supported Cu-based nanowire arrays as noble-metal free electrocatalysts for oxygen evolution. ChemSusChem 9:1–6
20. Huan TN, Rousse G, Zanna S, Lucas IT, Xu XZ, Menguy N, Mougel V, Fontecave M (2017) A dendritic nanostructured copper oxide electrocatalyst for the oxygen evolution reaction. Angew Chem Int Ed 56:4792–4796
21. Xu H, Feng JX, Tong YX, Li GR (2017) Cu_2O-Cu hybrid foams as high-performance electrocatalysts for oxygen evolution reaction in alkaline media. ACS Catal 7:986–991
22. Zhang BW, Li CJ, Yang G, Huang K, Wu JS, Li Z, Cao X, Peng DD, Hao SJ, Huang YZ (2018) Nanostructured CuO/C hollow shell@3D copper dendrites as a highly efficient electrocatalyst for oxygen evolution reaction. ACS Appl Mater Interfaces 10:23807–23812
23. Ren X, Ji XQ, Wei YC, Wu D, Zhang Y, Ma M, Liu ZA, Asiri AM, Wei Q, Sun XP (2018) In situ electrochemical development of copper oxide nanocatalysts within a TCNQ nanowire array: a highly conductive electrocatalyst for the oxygen evolution reaction. Chem Commun 54:1425–1428
24. Wu JX, He CT, Li GR, Zhang JP (2018) An inorganic-MOF-inorganic approach to ultrathin CuO decorated Cu-C hybrid nanorod arrays for an efficient oxygen evolution reaction. J Mater Chem A 6:19176–19181
25. Xiong XL, You C, Liu ZA, Asiri AM, Sun XP (2018) Co-doped CuO nanoarray: an efficient oxygen evolution reaction electrocatalyst with enhanced activity. ACS Sustain Chem Eng 6:2883–2887
26. Ding Y, Chen MW, Erlebacher J (2014) Metallic mesoporous nanocomposites for electrocatalysis. J Am Chem Soc 126:6876–6877
27. Chen Q, Ding Y, Chen MW (2018) Nanoporous metal by dealloying for electrochemical energy conversion and storage. MRS Bull 43:43–48
28. Lu Q, Hutchings GS, Yu WT, Zhou Y, Forest RV, Tao RZ, Rosen J, Yonemoto BT, Cao ZY, Zheng HM, Xiao JQ, Jiao F, Chen JG (2015) Highly porous non-precious bimetallic electrocatalysts for efficient hydrogen evolution. Nat Commun 6:6567
29. Li YX, Ge XB, Wang LDY, Liu J, Wang Y, Feng LX (2017) A free standing porous Co/Mo architecture as a robust bifunctional catalyst toward water splitting. RSC Adv 7:11568–11571
30. Zhang JT, Liu PP, Ma HY, Ding Y (2007) Nanostructured porous gold for methanol electro-oxidation. J Phys Chem C 28:10382–10388
31. Xu CX, Wang RY, Chen MW, Zhang Y, Ding Y (2010) Dealloying to nanoporous Au/Pt alloys and their structure sensitive electrocatalytic properties. Phys Chem Chem Phys 12:239–246
32. Ding Y, Chen MW (2009) Nanoporous metals for catalytic and optical applications. MRS Bull 34:569–576
33. Tan YW, Wang H, Liu P, Shen YH, Cheng C, Hirata A, Fujita T, Tang Z, Chen MW (2016) Versatile nanoporous bimetallic phosphides towards electrochemical water splitting. Energy Environ Sci 9:2257–2261

34. Liang FL, Yu Y, Zhou W, Xu XY, Zhu ZH (2015) Highly defective CeO_2 as a promoter for efficient and stable water oxidation. J Mater Chem A 3:634–640
35. Akhavan O, Azimirad R, Safa S, Hasani E (2011) CuO/$Cu(OH)_2$ hierarchical nanostructures as bactericidal photocatalysts. J Mater Chem 21:9634–9640
36. Lu CH, Qi LM, Yang JH, Zhang DY, Wu NZ, Ma JM (2004) Simple template-free solution route for the controlled synthesis of $Cu(OH)_2$ and CuO nanostructures. J Phys Chem B 108:17825–17831
37. Biesinger MC, Lau LWM, Gerson AR, Smart RSC (2010) Resolving surface chemical states in XPS analysis of first row transition metals, oxides and hydroxides: Sc, Ti, V, Cu and Zn. Appl Surf Sci 257:887–898
38. Deroubaix G, Marcus P (1992) X-ray photoelectron spectroscopy analysis of copper and zinc oxides and sulphides. Surf Interface Anal 18:39–46
39. Marshall AT, Vaisson-Béthune L (2015) Avoid the quasi-equilibrium assumption when evaluating the electrocatalytic oxygen evolution reaction mechanism by Tafel slope analysis. Electrochem Commun 61:23–26
40. Rossmeisl J, Qu ZW, Zhu H, Kroes GJ, Nørskov JK (2007) Electrolysis of water on oxide surfaces. J Electroanal Chem 607:83–89
41. Man IC, Su HY, Calle-Vallejo F, Hansen HA, Martínez JI, Inoglu NG, Kitchin J, Jaramillo TF, Nørskov JK, Rossmeisl J (2011) Universality in oxygen evolution electrocatalysis on oxide surfaces. ChemCatChem 3:1159–1165
42. Handoko AD, Deng SZ, Deng YL, Cheng AWF, Chan KW, Tan HR, Pan YL, Tok ES, Sow CH, Yeo BS (2016) Enhanced activity of H_2O_2-treated copper(II) oxide nanostructures for the electrochemical evolution of oxygen. Catal Sci Technol 6:269–274
43. Deng YL, Handoko AD, Du YH, Xi SB, Yeo BS (2016) In situ raman spectroscopy of copper and copper oxide surfaces during electrochemical oxygen evolution reaction: identification of Cu^{III} oxides as catalytically active species. ACS Catal. 6:2473–2481